Formatted: Numbering: Continuous

ICESat-2/ATLAS Instrument Linear System Impulse Response

Christopher T. Field[1,2†], Anthony J. Martino[2], and Luis Ramos-Izquierdo[2]

[1]Hexagon US Federal, Chantilly, VA, United States

[2]NASA Goddard Space Flight Center, Greenbelt, MD, United States.

Corresponding author: Christopher T. Field (Christopher.T.Field@NASA.gov) and Anthony. J. Martino (Anthony.J.Martino@NASA.gov)

†Now at Aurora Engineering, Orono, ME, United States

Key Points:

- ICESat-2 instrument impulse response contains predictable afterpulses
- Afterpulses can be used to estimate characteristics of distorted first pulses

Abstract

Ideally, the response of the Advanced Topographic Laser Altimeter System (ATLAS) instrument on the Ice, Cloud, and land Elevation Satellite–2 (ICESat-2) observatory to returns from a flat target at a fixed distance would be a single peak. However, ICESat-2 profiles from very flat surfaces display extra features below the presumed Earth surface. This paper identifies the multiple reflections within the ATLAS receiver that create those extra pulses. We describe their sources, compare their measured position to optical ray trace predictions, and discuss their relative amplitude. We then explore the possibility of using afterpulses to extract surface elevation information from highly saturated returns, in which the first return pulse is distorted and displaced by nonlinear effects in the detector.

1 Introduction

The Advanced Topographic Laser Altimeter System (ATLAS) instrument on the Ice, Cloud, and land Elevation Satellite–2 (ICESat-2) observatory uses laser light and single-photon-sensitive photomultipler tubes to measure surface elevation (Martino, et al., 2019; Neumann, et al., 2019). The cited papers describe the design and operation of ATLAS. This paper provides a closer look at one particular characteristic of the instrument that has produced artifacts visible in on-orbit data: its linear system impulse response.

ATLAS provides for monitoring changes in start or receiver signal delays and impulse response shapes by routing a very small amount of the outgoing laser light through optical fibers, called the Transmitter Echo Path (TEP), to detectors for two of the six beams (on two of the three photon-counting electronics cards). The intensity of light through this path has been adjusted so that one photon is detected about every 10 to 20 laser shots. The times of flight of TEP photons are measured from the same start pulse as times of flight of return photons, so changes in TEP time of flight can be used to correct for gradual changes in the bias of return times of flight. Many hundreds of TEP photons (many thousands of shots) are required to yield millimeter-range precision.

Multiple reflections in the receiver system result in some collected photons arriving at the detectors “late”. Thus the impulse responses for TEP and return contain several afterpulses in addition to the first pulse. The afterpulses can appear as a false surface under the true surface when the terrain is very flat, over water surfaces, or especially when specular surface reflections generate very strong returns.

Because the optical paths for TEP photons and return photons are different, the impulse responses for the two photon sources are also slightly different. This paper reports on the ATLAS system impulse responses both sources of photons, and it describes the locations and amplitudes of the afterpulses relative to the first pulse.

Time-of-flight values from multiple shots are often aggregated in a histogram to produce a waveform-like display. The background photoevent rate can be estimated as the base or floor of the histogram. The location of scattering targets can be identified as peaks, also referred to as “pulses” in this paper. The minimum pulse width is the transmitted pulse width, about 1.25 ns; surface roughness often widens it. A fit to an exponentially-modified Gaussian (EMG) function is used to extract a single time of flight from each peak/pulse. (Greeley et. al, 2019; Lacouture & Cousineau, 2008; Roland, 1985)

2 System Impulse Response

2.1 System Impulse Response

Figure 1a shows the ATLAS small-signal (single photon per shot) response to a flat target, in this case the a lateral-transfer retroreflector called the Zero-Range Target that was used during pre-launch Integration and Test (I&T) to calibrate the absolute range measurement. The first big peak is the return from the Zero Range Target (1.5 photoevents from the target per shot), while the second, third, and (very small) fourth peaks (AP 1, AP 2, and AP3) are afterpulses generated by optical reflections in the ATLAS receiver system. The solid red line is three Exponentially Modified Gaussian functions plus a constant fit to the background level. The histogram is computed in 50-ps bins and smoothed over 7 bins (a 350-ps window).

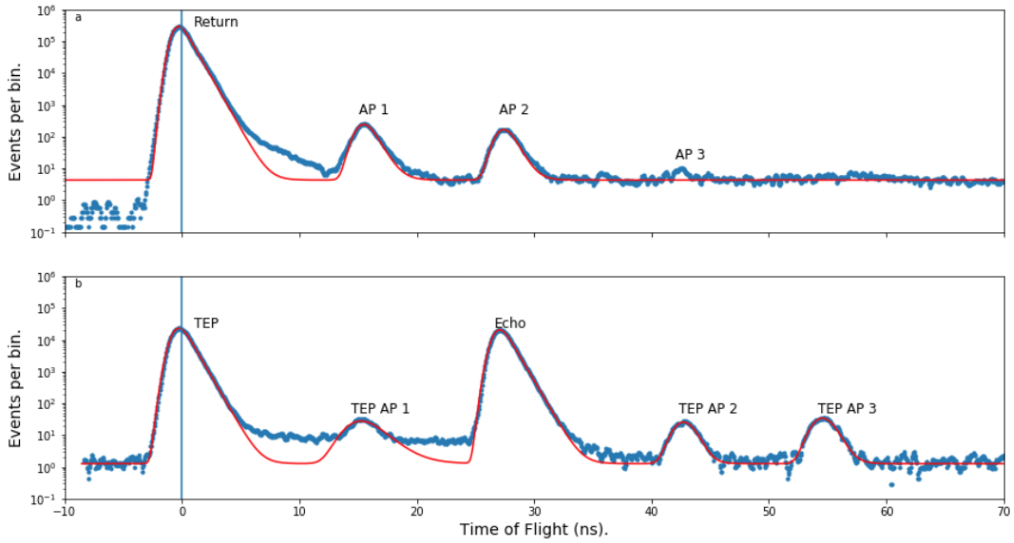

Figure 1. Small-signal system impulse response data collected for 10 minutes during integration and testing on 2 March 2016 starting at 19:50 during the Zero-Range Test. (a) Beam 3 response from surface reflections (blue dots) with three fitted Exponentially Modified Gaussian functions (red line), showing the first pulse and afterpulses. The elevated background level lasts for several hundred ns. (b) Beam 1 TEP response.

There are four features of particular note. First, after the first pulse there are two nearly equal-amplitude afterpulses about the same shape as the first pulse, although three to four orders of magnitude weaker than the first pulse. Second, the histogram floor (background) is different before the first pulse than between or after the pulses. This suggests that the ATLAS detectors have a long tail of internally generated events generated at random times, or, less likely, there is some residual laser emission after the main laser pulse. This has implications for estimation of background solar rate as it is traditional to define the background as the event rate from "below" the ground because that would normally ensure there was no atmosphere backscattered laser

light. Third, the received pulse shape seems to be described well as an Exponentially Modified Gaussian plus an exponentially decaying component, which we have not tried to model as it starts more than three orders of magnitude below the peak. Fourth, the fitting function we used sets the same background rate before and after the pulse.

Figure 1b shows the TEP system impulse resonse. The third pulse, which we call “Echo”, is nearly the same amplitude as the intial pulse and is followed by two more afterpulses.

The histograms shown in Figure 1 were taken at the same time with the slightly more than 7 million shots in the data set. The horizontal axis of each plot has been adjusted so that the first peak's centroid is at the origin. The TEP peak is about an order of magnitude smaller than Return peak from the Zero-Range Target. This difference in incident photon rate might explain why the floor in Figure 1b returns to its previous level while the floor in Figure 1a does not.

These responses were measured using detector bank B (Detector Bank A has been in use continuously during the first two years in orbit) and the original lasers, which were replaced before launch. However, the data still accurately describes the instrument's behavior on orbit.

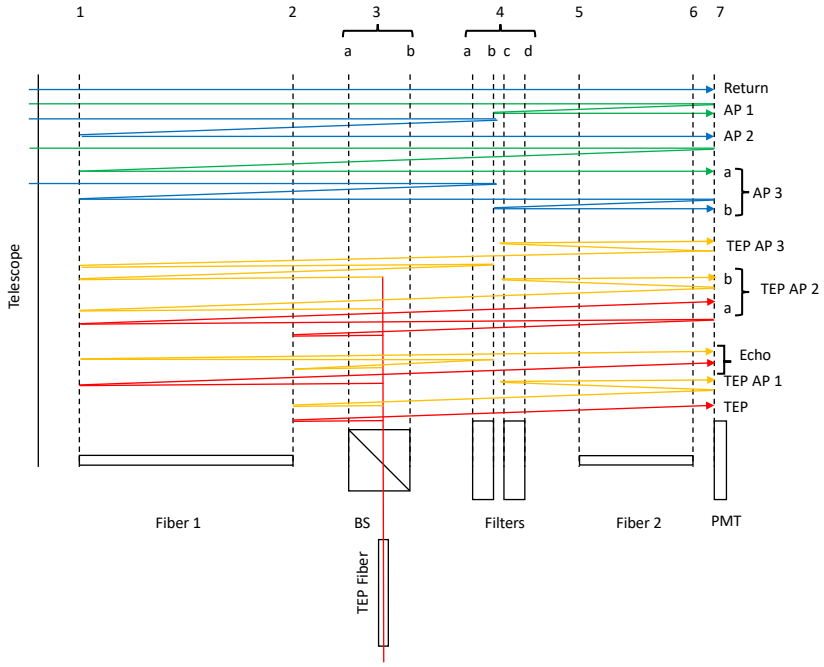

Figure 2. Schematic showing the receiver optical paths that produce the surface return and its afterpulses and the TEP, Echo, and their afterpulses. Some optical surfaces that do not contribute to observed effects are omitted for clarity.

2.2 Surface return receiver optical system

The top half of Figure 2 shows the multiple paths within the ATLAS receiver system that ground return photons follow from the telescope to the detector, creating the first pulse and several afterpulses. There are four optical components of interest: fiber 1(with ends at planes 1 and 2) between the telescope and the receiver optical bandpass filters, the bandpass filters (planes 4a-d), fiber 2 between the filters and the detectors (with ends at planes 5 and 6), and the photomultiplier detectors (plane 7).

Light from the surface is collected by the telescope and conveyed by fiber 1 to the optical bandpass filters. While the filters reflect about 30% of the in-band light back toward the telescope, most of the light continues through fiber 2 to the detector where it generates the first pulse. This is the path depicted in blue by the top path in Figure 2. At the detector, about 85% of the incident light is reflected back through fiber 2 to the filters. In the filter assembly, several surfaces reflect some of this light back to the detector producing the first afterpulse (AP 1). This is the second path, in green, shown in Figure 2. Because there are several reflective surfaces, AP 1 is a bit wider than the initial return. The second afterpulse (AP 2) is generated by the light initially reflected from the filters into fiber 1 and reflected at plane 1 by the fiber end, shown in blue as the third line in Figure 2. Afterpulse 3 is a composite of light that traveled by either of two paths (AP 3a and AP 3b) through both fibers a total of 3 times.

The strength of each afterpulse relative to the first pulse depends on the reflectance of each surface. The most variable reflectance values are at the antireflection (AR) coated fiber faces at plane 1, 2, 5, and 6, which have specified transmittance greater than 99%. The reflectance could vary over half an order of magnitude between components, but are expected to be constant over time. The fiber end at plane 1 (which generates AP 2 and AP 3 is the only one that directly impacts the relative amplitude of the afterpulses documented here.

Variations in the lengths of each beam's fibers cause the afterpulse intervals to be different for each of the 6 beams. Also, differences in the the precise value of reflectance at each surface (particularly antireflection-coated surfaces) make the magnitudes of the afterpulses relative to the first pulse different for each beam.

2.3 TEP receiver optical system

In the return path of the strong beams 1 and 3, a weak sample of the outgoing laser pulse is directed from the TEP fiber shown at the bottom of Figure 2 toward the beamsplitter, which reflects about 1% of the TEP fiber output to the input face of Fiber 1 (plane 2), from which less than 1% of the light reflects to generate the first pulse, designated TEP, corresponding to the first peak in Figure 1b. This path is shown in bottom red path in Figure 2. In the next path, shown in yellow, second line from bottom, some of the light is reflected off the detector face, passes through fiber 2 and is reflected off the filters to generate TEP AP 1, with the same interval between TEP and TEP AP1 as between Return and AP 1.

Most of the light directed by the beamsplitter toward the telescope passes through fiber 1, as shown in red third line, where less than 1% is reflected at plane 1 back toward the detector where it generates the "Echo" pulse. The relative strength of the TEP and Echo is strongly dependent on the reflectivity of each end of fiber 1. There is an additional path, in yellow, that arrives slightly later than the Echo, but, because it experiences two fiber end reflections, is at most 1% of the Echo pulse and can be ignored. Note that the interval between the TEP and Echo

is defined by the length of fiber 1 (planes 1 and 2), while the interval between Return and AP 2 is defined by the slightly longer distance between planes 1 and 4. The difference is visible in Figure 1.

The light reflected at plane 1 arrives like a ground return, generating two afterpulses analogous to AP 2 and AP 3. AP 2 also overlaps light that is initially reflected at plane 2 and then makes two passes through fiber 1 and three passes through fiber 2.

2.3 Comparison of modeled and measured delays

During a part of ATLAS thermal-vacuum testing, between 10 January and 12 January 2018, there was a temperature transition during which ATLAS was operating in the post-launch configuration: Laser 2, Start Pulse Detector A, and photon-counting Detector Bank A. Taking a portion of the data collected, computing the pulse centroids from the EMG fits, and averaging over the 6 beams yields the nominal afterpulse intervals given in Table 1, which also lists the ray-trace predicted intervals. Taking the ratio of the total number of events in each pulse to the total events in the first pulse yields the measured afterpulse relative strengths, which are given along with the ray trace predictions. The ray trace model assumed that light travels through straight optical fibers; the transit time through the actual fibers, which curve around bends, is slightly different (tens of picoseconds per meter) due to different mode distributions. The qualitative similarity of the intervals and ratios suggests we have correctly identified the important reflective surfaces.

	Time from first pulse to afterpulse (ns)		Ratio of total afterpulse events to first pulse events	
	Measured	Model	Measured	Model
AP 1	15.4	14.5	1.9e-3	3.1e3
AP 2	27.9	27.3	6.9e-4	3.1e-3
AP 3	43.0	41.7	7.4e-6	4.1e-5
TEP AP 1	15.5	14.5	1.5e-3	2.9e-3
Echo	27.1	27.0	6.5e-1	7.3e-1
TEP AP 2	42.5	41.5	5.7e-4	2.2e-3
TEP AP 3	54.3	54.0	1.0e-3	3.5e-3

Table 1. Comparison of the nominal time interval between the ground return and its afterpulses and the TEP and its afterpulses as observed and predicted by optical ray trace. Return intervals/ratios collected 11 January 2018 from 02:16 to 05:15.

3 Precise afterpulse intervals and ratios

Having correctly identified the afterpulse sources, they can be appropriately flagged in the ICESat-2 ATL03 data product (Neumann, T. A et al. 2020). However, a more precise

description of the afterpulse intervals and ratios may permit recovery of surface elevation from returns too distorted by dead-time effects to be accurately measured.

Near-specular returns from flat, smooth surfaces can contain so many photons that many of them arrive during receiver's dead time after the first photon detection. The result is that the time-of-flight histogram of the first return is highly distorted (in some extreme cases even bifurcated), and its centroid is displaced toward the leading edge by an unknown amount. The afterpulses, which are several orders of magnitude weaker than the first pulse, are not so distorted or displaced. Thus, they may provide a means by which the location and strength of the first pulse can be estimated if the relationship between the first pulse and the afterpulses is known well enough.

With that goal in mind, in Table 2 we report for each beam the interval between the first pulse and each afterpulse and the ratio of the number of events in each afterpulse to the main pulse.

Return	1st Afterpulse Delay (ns)	1st Afterpulse Ratio	2nd Afterpulse Delay (ns)	2nd Afterpulse Ratio	3rd Afterpulse Delay (ns)	3rd Afterpulse Ratio		
1	15.47	0.0013	27.91	0.00076	43.17	6e-6		
2	15.21	0.0012	27.83	0.00019	43.77	1e-6		
3	15.63	0.00095	27.66	0.00058	42.43	1e-6		
4	15.53	0.0016	28.04	0.00072	42.08	7e-6		
5	15.41	0.0017	28.04	0.00080	43.16	1e-6		
6	15.46	0.0026	28.01	0.0011	43.25	2.8e-5		
TEP	1st Afterpulse Delay (ns)	1st Afterpulse Ratio	Echo Pulse Delay (ns)	Echo Pulse Ratio	2nd Afterpulse Delay (ns)	2nd Afterpulse Ratio	3rd Afterpulse Delay (ns)	3rd Afterpulse Ratio
1	15.49	1.9e-3	27.33	0.86	42.72	8.8e-4	54.57	1.5e-3
3	15.52	1.2e-3	26.88	0.45	42.41	2.6e-4	53.99	5.7e-4

Table 2. For each beam, the time interval between the first pulse centroid and each afterpulse centroid and the fraction of the first pulse events present in each afterpulse. The interpulse time and afterpulse ratios are median values. Uncertainties in interpulse intervals are ±50 ps and uncertainties in the ratios are ±2 in the last significant digit.

4 Conclusions

The ATLAS system impulse response has several extra peaks that complicate interpretation of returns from flat surfaces by forming a “shadow” of the surface some distance below it. We have identified the internal reflecting surfaces that generate those extra features, and we have shown that their location as predicted by ray traces of the receiver optical system matches the measured intervals.

We propose that over specular surfaces, these attenuated copies of the surface return could be used to recover estimated surface elevations even when the initial return is too saturated to yield a useful pulse shape. To that end, we have presented the interval between the initial ground return and each afterpulse to 50 ps and reported the ratio of the number of photoevents in each afterpulse to the number in the first pulse.

Acknowledgments, Samples, and Data

Funding was provided by the NASA ICESat-2 Project Science Office. We thank the ATLAS integration and test team for the pre-launch data that we used. The source data files for this work are available on the ICESat-2 website (https://icesat-2.gsfc.nasa.gov).

References

Greeley, A. P. Neumann, T. A., Kurtz, N. T., Markus, T., & Martino, A. J. (2019), Characterizing the System Impulse Response Function From Photon-Counting LiDAR Data. *IEEE TRANSACTIONS ON GEOSCIENCE AND REMOTE SENSING*, *57*(9), 6542–6551. doi: 10.1109/TGRS.2019.2907230

Lacouture, Y., & Cousineau, D. (2008), How to use MATLAB to fit the ex- Gaussian and other probability functions to a distribution of response times. *Tuts. Quant. Methods Psychol*, *4*(1), 35–45.

Martino, A. J., Neumann, T. A., Kurtz, N. T., McLennan, D ., (2019), ICESat-2 mission overview and early performance. *Proc. SPIE 11151, Sensors, Systems, and Next-Generation Satellites, XXIII* (10),. doi: https://doi.org/10.1117/12.2534938

Neumann, T. A., Martino, A. J., Markus, T., Bae, S., Bock, M. R., Brenner, et al. (2019) , The Ice, Cloud, and Land Elevation Satellite – 2 mission: A global geolocated photon product derived from the Advanced Topographic Laser Altimeter. *Remote Sensing of Environment*, *233*. doi: 10.1016/j.rse.2019.111325

Neumann, T. A., Brenner, A, Hancock, D., Robbins, J., Saba, J., Harbeck, et al. (2020) , *ATLAS/ICESat-2 L2A Global Geolocated Photon Data, Version 3.. Boulder, Colorado USA. NASA National Snow and Ice Data Center Distributed Active Archive Center*. doi: https://doi.org/10.5067/ATLAS/ATL03.003

Roland, D. (1985), Series for the exponentially modified Gaussian peak shape. *Analytical Chemistry*, *57*(1), 388–388. doi: 10.1021/ac00279a094